OncoTargets and Therapy Dovepress

Open Access Full Text Article ORIGINAL RESEARCH

Identification of Potential Biomarkers in Papillary Thyroid Carcinoma Based on Proteomics

Yu Sun[1,*], Jiaxuan Sun[1,*], Xiaona Gao[1], Tiefeng Shi[1], Maoqing Wang[2]

[1]Department of Thyroid Surgery, The Second Affiliated Hospital, Harbin Medical University, Harbin, People's Republic of China; [2]Department of Nutrition and Food Hygiene, School of Public Health, Harbin Medical University, Harbin, People's Republic of China

*These authors contributed equally to this work

Correspondence: Tiefeng Shi, Department of Thyroid Surgery, The Second Affiliated Hospital, Harbin Medical University, Harbin, People's Republic of China, Email shitiefeng1970@163.com; Maoqing Wang, Department of Nutrition and Food Hygiene, School of Public Health, Harbin Medical University, Harbin, People's Republic of China, Tel +86-451-87502876, Fax +86-451-87502885, Email wang_maoqing@126.com

Background: To identify biomarkers of papillary thyroid carcinoma (PTC) and explore the possible pathogenic mechanism.

Methods: This study included five patients with PTC. Protein expression of cancer tissues and adjacent normal thyroid tissues from each patient were analyzed by TMT proteomics technology. Differentially expressed proteins were identified, and functional annotation of differentially expressed proteins was performed by bioinformatics and pathway enrichment analysis.

Results: A total of 639 differentially expressed proteins were identified, including 278 upregulated and 361 downregulated proteins. Six upregulated proteins were identified as potential specific markers of PTC.

Conclusion: Differentially expressed proteins may represent new molecular markers of PTC. These differentially expressed proteins and the related pathways may provide new insights into the pathogenic mechanisms of PTC.

Keywords: papillary thyroid carcinoma, TMT, proteomics, PRM, molecular markers

Introduction

Thyroid cancer is a relatively common endocrine system disease that tends to affect younger individuals, and its incidence is gradually increasing worldwide, including in China.[1–4] The most common pathological type of thyroid cancer is papillary thyroid carcinoma (PTC), accounting for about 85% of all thyroid cancers.[5]

The 2015 American Thyroid Association guidelines currently recommend active surveillance for patients with low-risk papillary thyroid carcinoma. Ultrasound-guided ablation has also been used to treat low-risk papillary thyroid carcinoma and achieved good results.[6–8] However, some PTCs are highly invasive, and local and distant metastases can occur in the early stage. If not treated in time, PTC can seriously affect patient prognosis and even endanger life. The current diagnostic methods for papillary thyroid carcinoma are not sufficiently accurate. Furthermore, symptoms at the early stage are not obvious, and most patients have already reached the advanced stage at diagnosis, which leads to poor prognosis. Therefore, identifying a new method for early diagnosis and prognosis evaluation of PTC is critical.

While the accuracy of lymph node diagnosis with ultrasound is high, the diagnostic sensitivity for central compartment lymph node metastasis (CLNM) is only 10.9% to 36.2%.[9] Some surgeons still treat patients by surgical resection. Central compartment lymph node dissection (CLND) reduces the tumor recurrence rate and improves the TNM staging of some patients.[10] Preventive CLND increases the risk of surgical complications including recurrent laryngeal nerve injury, parathyroid injury and other surgical complications.[11]

In this study, we used proteomics to search for potential specific and sensitive biomarkers for PTC, which can aid in the improvement of the early diagnosis rate of PTC. The analysis of differential protein metabolic pathways in PTC may also provide new insights into the pathogenesis of PTC.

Received: 1 June 2024
Accepted: 10 October 2024
Published: 3 November 2024

Materials and Methods

Patients and Specimens

This study was approved by the ethics committee of The Second Affiliated Hospital of Harbin Medical University and all patients have agreed with and signed on the consent form before. Thyroid cancer tissue and adjacent normal tissue samples were collected from patients undergoing surgical resection in the Department of Thyroid Surgery, The Second Affiliated Hospital of Harbin Medical University from January 2020 to January 2021. Inclusion criteria were as follows: (1) subtotal or total thyroidectomy was performed in the thyroid surgery department of the Second Affiliated Hospital of Harbin Medical University, and lymph node dissection in the central region of the neck (region VI and region VIII) was performed during the operation; (2) postoperative pathology confirmed as single-focal PTC; and (3) ultrasound examination of the thyroid in the Second Affiliated Hospital of Harbin Medical University within 2 months before operation with complete image information. Exclusion criteria were as follows: (1) lymph node skip metastasis occurred, that is, lymph node metastasis in the lateral neck region but no lymph node metastasis in the central region; (2) postoperative pathology showed multifocal PTC; (3) case data were incomplete; and (4) Hashimoto's disease. Finally, a total of five patients were included, including two men and three women. The surgical specimens were put into labeled cryopreservation tubes and immediately placed in liquid nitrogen, and the tubes were transferred to a −80°C freezer for storage. The staging standard is in accordance with the TNM staging of the International Union Against Cancer (UICC) (Table 1).

HE Staining

The surgical sections of the five patients were stained in hematoxylin solution for several minutes and then placed in acid water and ammonia water for color separation for a few seconds. The samples were rinsed with running water for 1 h and then put into distilled water. The samples were dehydrated in 70% and 90% alcohol for 10 min each. The samples were then stained with alcohol eosin staining solution for 2–3 min.

Protein Extraction

Samples were ground into fine powder with a mortar in liquid nitrogen. Next, 500 μL of SDT lysate was added to resuspend the precipitate, followed by vortexing and heading in boiling water for 5 min. Ultrasonic crushing was performed (80W, 10s on, holding for 15s, 10 times) and then samples were heated in a boiling water bath for 15 min. The sample was centrifuged at 14000 g for 40 min; the supernatant was filtered with a 0.22 μm membrane filter and the filtrate was collected. The concentration and quality of the extracted protein were determined and evaluated by BCA method and SDS-PAGE gel electrophoresis.

Enzymatic Hydrolysis and Peptide Desalting

Peptides (200 μg) were taken from each sample for enzymatic digestion before 100 mm DTT was added. The samples were boiled in a water bath for 5 min and cooled to room temperature. Next, 200 μL UA buffer (8 M urea, 150 mm Tris-HCl, pH 8.0) was added and the sample was mixed. The samples were transferred to a 10KD ultrafiltration centrifuge tube and centrifuged at 12000 g for 15 min. Next, 200 μL UA buffer was added and the sample was centrifuged at 12000 g for 15 min; the filtrate was discarded. Next, 100 μL IAA (50 mm IAA in UA) was added and the mixture was shaken at 600 rpm for 1 min and held at room temperature for 30 min protected from the light, followed by centrifugation at 12000 g for 10 min. Next, 100 μL UA buffer was added and the sample was centrifuged at 12000 g for 10 min; this procedure

Table 1 The Specific Case Information Data of 5 Specimens

Number	Gender	Age	Left/Right	Stage	Lymphatic Metastasis	Distant Metastasis	TNM	Histology
1	Male	43	L	T1b	N1a	M0	I	PTC
2	Male	32	R	T1a	N1a	MO	I	PTC
3	Female	57	R	T1a	N0	MO	I	PTC
4	Female	45	L	T1a	N0	M0	I	PTC
5	Female	65	R	T1b	N0	M0	I	PTC

was repeated twice. NH_4HCO_3 (100 μL) buffer was added, and the sample was centrifuged at 14000 g for 10 min; this was repeated twice. Trypsin buffer (6 μg trypsin in 40 μL NH_4HCO_3 buffer) was added and the sample was shaken at 600 rpm for 1 min and incubated at 37°C for 16–18 h. The collection tube was replaced with a new one and the sample was centrifuged at 12000 g for 10 min. The filtrate was collected and 0.1% TFA solution was added, followed by desalting with the C18 Cartridge. The peptides were then quantified.

TMT Marking and Grading

Sample Preparation

For tissue lysis, tissue was suspended on ice in 200 μL lysis buffer (4% SDS, 100 mm DTT, 150 mm Tris-HCl pH 8.0). Tissue was disrupted with agitation using a homogenizer, and boiling for 5min. The samples were further ultrasonicated and boiling again for another 5 min. Undissolved cellular debris were removed by centrifugation at 16000 rpm for 15 min. The supernatant was collected and quantified with a BCA Protein Assay Kit (Bio-Rad, USA).

Protein Digestion

Digestion of protein (200 μg for each sample) was performed according to the FASP procedure described by Wisniewski, Zougman et al. Briefly, the detergent, DTT and other low-molecular-weight components were removed using 200 μL UA buffer (8 M Urea, 150 mm Tris-HCl pH 8.0) by repeated ultrafiltration (Microcon units, 30 kD) facilitated by centrifugation. Then 100 μL 0.05 M iodoacetamide in UA buffer was added to block reduced cysteine residues and the samples were incubated for 20 min in darkness. The filter was washed with 100 μL UA buffer three times and then 100 μL 25 mm NH4HCO3 twice. Finally, the protein suspension was digested with 4 μg trypsin (Promega) in 40 μL 25 mm NH4HCO3 overnight at 37 °C, and the resulting peptides were collected as a filtrate. The peptide concentration was determined with OD280 by Nanodrop device.

TMT Labeling of Peptides

Peptides were labeled with TMT reagents according to the manufacturer's instructions (Thermo Fisher Scientific). Each aliquot (100 μg of peptide equivalent) was reacted with one tube of TMT reagent, respectively. After the sample was dissolved in 100 μL of 0.05M TEAB solution, pH 8.5, the TMT reagent was dissolved in 41 μL of anhydrous acetonitrile. The mixture was incubated at room temperature for 1 h. Then 8μL of 5% hydroxylamine to the sample and incubate for 15 minutes to quench the reaction. The Multiplex labeled samples were pooled together and lyophilized.

LC-MS/MS Analysis

LC- MS analysis was performed on a Q Exactive mass spectrometer that was coupled to Easy nLC (Thermo Fisher Scientific). Peptide from each fraction was loaded onto a the C18-reversed phase column (12cm long, 75μm ID, 3μm) in buffer A (2% acetonitrile and 0.1% Formic acid) and separated with a linear gradient of buffer B (90% acetonitrile and 0.1% Formic acid) at a flow rate of 300 nL/min over 90 min. The linear gradient was set as follows: 0–2 min, linear gradient from 2% to 5% buffer B; 2–62 min, linear gradient from 5% to 20% buffer B; 62–80 min, linear gradient from 20% to 35% buffer B; 80–83 min, linear gradient from 35% to 90% buffer B; 83–90 min, buffer B maintained at 90%. MS data was acquired using a data-dependent top15 method dynamically choosing the most abundant precursor ions from the survey scan (300–1800 m/z) for HCD fragmentation. Determination of the target value is based on predictive Automatic Gain Control (pAGC). The AGC target values of 1e6, and maximum injection time 50 ms were for full MS, and a target AGC value of 1e5, maximum injection time 100 ms for MS2. Dynamic exclusion duration was 30s. Survey scans were acquired at a resolution of 70,000 at m/z 200 and resolution for HCD spectra was set to 35,000 at m/z 200. Normalized collision energy was 30. The instrument was run with peptide recognition mode enabled.

Database Searching and Analysis

The resulting LC-MS/MS raw files were imported into Proteome Discoverer 2.4 software (version 1.6.0.16) for data interpretation and protein identification against the database Uniprot_Hordeum-vulgare_201747-20180125 (downloaded on

25/01/2018, and including 201747 protein sequences), which is sourced from the protein database at https://www.uniprot.org/taxonomy9606. An initial search was set at a precursor mass window of 10 ppm. The search followed an enzymatic cleavage rule of Trypsin/P and allowed maximal two missed cleavage sites and a mass tolerance of 20ppm for fragment ions.

Data Processing and Bioinformatics Analysis

Analyses of bioinformatics data were carried out with Perseus software, Microsoft Excel and R statistical computing software. Differentially significant expressed proteins were screened with the cutoff of a ratio fold-change of >1.20 or <0.83 and P-values < 0.05. Expression data were grouped together by hierarchical clustering according to the protein level. To annotate the sequences, information was extracted from UniProtKB/Swiss-Prot, Kyoto Encyclopedia of Genes and Genomes (KEGG), and Gene Ontology (GO). GO and KEGG enrichment analyses were carried out with the Fisher's exact test, and FDR correction for multiple testing was also performed. GO terms were grouped into three categories: biological process (BP), molecular function (MF), and cellular component (CC). Enriched GO and Kegg pathways were nominally statistically significant at the $p<0.05$ level. Construction of protein–protein interaction (PPI) networks were also conducted by using the STRING database with the Cytoscape software.

PRM Verification of Differential Protein Expression

Sample Information

Sample quantity: 10 cases, information is shown in Table 2. The number of target proteins in this PRM experiment is 20, and the specific peptide segments are shown in Table 3 of the attachment.

To verify the protein expression levels obtained by TMT analysis, the expression levels of selected proteins were further quantified by LC-PRM/MS. Briefly, peptides were prepared according to the TMT protocol. Tryptic peptides were loaded on C18 stage tips for desalting prior to reversed-phase chromatography on an Easy nLC-1200 system (Thermo Scientific). One hour liquid chromatography gradients with acetonitrile ranging from 5 to 35% in 45 min were used. PRM analysis was performed on a Q Exactive Plus mass spectrometer (Thermo Scientific). Methods optimized for collision energy, charge state, and retention times for the most significantly regulated peptides were generated experimentally using unique peptides of high intensity and confidence for each target protein. The mass spectrometer was operated in positive ion mode and with the following parameters: The full MS1 scan was acquired with the resolution of 70000 (at 200 m/z), automatic gain control (AGC) target values 3.0×10^6, and a 250 ms maximum ion injection times. Full MS scans were followed by 20 PRM scans at 35000 resolution (at m/z 200) with AGC 3.0×10^6 and maximum injection time 200ms. The targeted peptides were isolated with a 2Th window and fragmented at normalized collision energy of 27 in a higher energy dissociation (HCD) collision cell. The raw data were analyzed using Skyline (MacCoss Lab, University of Washington) to get the signal intensities of individual peptide sequences.

For PRM MS data, each sample's average base peak intensity was extracted from the full scan acquisition using RawMeat (version 2.1, VAST Scientific, www.vastscientific.com). The normalization factor for sample N was calculated as f_N= the average base peak intensity of sample N/the median of average base peak intensities of all samples. The area under curve (AUC) of each transition from sample N was multiplied by this factor. After normalization, the AUC of each transition was summed to obtain AUCs at the peptide level. Relative protein's abundance was defined as the intensity of a certain peptide.

Using GO and KEGG and other bioinformatics analysis methods, proteins with potential biomarker significance related to papillary thyroid carcinoma were screened out. The expression levels of the proteins were verified using parallel reaction monitoring (PRM) technology.

Table 2 Samples in PRM Verification

Sample names				
A2 B2	A3 B3	A4 B4	A7 B6	A8 B7

Table 3 Targeted Peptide PRM Quantitative Skyline Analysis Table

Protein	A2	A3	A4	A7	A8	B2	B3	B4	B6	B7	FC (A.vs.B)	P-value(A.vs.B)
sp|O15230|LAMA5_HUMAN	131963697	91,082,804	176,569,391	156,916,520	115,444,997	154,205,023	124,291,213	82,749,554	166,863,174	89,279,105	1.0884198	0.641444582
sp|O75369|FLNB_HUMAN	120416619	52,397,130	85,243,975	74,609,453	65,293,668	57,587,830	43,469,560	34,772,303	79,079,655	31,810,800	1.6130051	0.069600275
sp|P01266|THYG_HUMAN	4.325E+09	5.745E+09	3.862E+09	1.972E+09	4.797E+09	1.254E+10	5.574E+09	7.099E+09	2.406E+09	8.325E+09	0.5758909	0.124821873
sp|P22748|CAH4_HUMAN	8971775.3	7,177,240.2	1,787,727.4	1,474,022.9	3,930,705.7	19,620,622	20,961,448	22,616,723	47,563,135	11,914,389	0.1902688	0.012736302
sp|P46109|CRKL_HUMAN	61776968	22,091,654	47,456,725	32,321,917	33,351,965	24,816,003	18,144,630	4,817,943.3	32,959,801	11,628,034	2.1328016	0.038701336
sp|Q07812|BAX_HUMAN	115503909	27,268,036	107,200,920	43,830,609	34,245,034	22,441,177	12,207,595	8,025,924.7	27,598,270	7,508,197.6	4.2175829	0.032138153
tr|A0A024R9Q1|A0A024R9Q1_HUMAN	376733695	139,165,352	83,651,673	84,375,937	63,968,708	6,808,490.1	10,034,472	5,213,610.1	4,898,923.3	14,210,623	18.167741	0.04123442
tr|A0A024RAQ9|A0A024RAQ9_HUMAN	190891861	101,158,328	89,635,093	150,216,481	273,671,117	12,574,107	12,563,072	6,692,015	40,951,624	13,461,967	9.3407568	0.002867457
tr|A0A140T9C0|A0A140T9C0_HUMAN	69124221	51,774,161	37,541,844	96,217,170	7,549,509.2	76,133,833	40,476,052	30,468,918	58,072,820	20,451,250	1.1622498	0.693249244
tr|A0A3B3ITK0|A0A3B3ITK0_HUMAN	166906185	105,943,442	24,347,342	45,799,690	40,214,200	176,670.77	315,174.02	155,726.89	1,219,788.5	582,614.86	156.41419	0.02063048
tr|B1PL87|B1PL87_HUMAN	57827106	12,853,870	43,982,796	26,912,493	16,771,505	11,415,667	5,002,701.5	3,349,141.3	6,693,016	3,418,564.9	5.2996181	0.017389311
tr|B2RCZ7|B2RCZ7_HUMAN	1.736E+09	222,829,306	2.258E+09	386,627,303	125,942,292	74,785,003	55,050,014	29,577,567	108,587,789	42,742,545	15.218599	0.078995646
tr|B4DG27|B4DG27_HUMAN	2005861.7	1,499,182.9	1,420,176.6	1,824,291.1	169,158.23	1,570,470.8	2,474,767.5	1,417,270.9	4,025,686.4	1,226,673	0.6457074	0.247832507
tr|B4DSW9|B4DSW9_HUMAN	59911898	22,503,696	44,741,791	34,603,092	33,714,390	31,584,953	24,255,162	16,116,260	46,254,028	17,108,970	1.4445446	0.189108649
tr|D6RGG3|D6RGG3_HUMAN	158889891	88,374,332	85,918,445	57,592,598	37,174,382	2,695,919.8	1,563,944.6	1,569,494.9	3,765,715.6	1,293,198.3	39.30372	0.003720185
tr|G3XAP6|G3XAP6_HUMAN	73806283	38,276,856	33,112,505	38,811,046	15,914,120	3,135,660.8	2,369,635.6	1,339,262.7	3,648,462.5	1,235,676.8	17.045439	0.004003304
tr|L7RT18|L7RT18_HUMAN	71643770	25,377,903	67,963,702	46,357,037	31,587,837	21,551,055	20,590,230	16,775,576	39,418,410	12,636,461	2.1891183	0.034737056
tr|Q59F15|Q59F15_HUMAN	194845939	178,124,917	221,923,231	196,176,830	358,001,048	307,099,139	173,493,257	111,453,405	169,536,323	120,562,453	1.3025892	0.297934221
tr|Q86TY5|Q86TY5_HUMAN	690816792	134,009,956	469,033,533	264,745,123	85,040,670	82,905,661	34,369,345	39,304,532	64,151,378	37,132,794	6.3740884	0.039352103
tr|R4GN98|R4GN98_HUMAN	1.094E+10	1.547E+09	1.464E+10	4.194E+09	2.816E+09	914,578,079	569,140,895	510,099,137	1.932E+09	673,350,271	7.4223877	0.049291448

https://doi.org/10.2147/OTT.S465636 DovePress

Statistical Methods

Statistical analysis was performed using SPSS software (version 16.0, Chicago, IL, USA). The data are expressed as mean ± standard deviation, and the differences between the two groups were analyzed by paired *t*-test and rank sum test. A two-tailed $p<0.05$ was considered statistically significant. The volcano map was produced on the basis of formal data for protein identification, and the statistics were calculated using a paired *T*-test.

Results

Confirmation of Papillary Thyroid Carcinoma

HE staining showed that the thyroid cells exhibited a papillary structure (Figure 1). These features are consistent with the typical pathological features of papillary thyroid carcinoma.

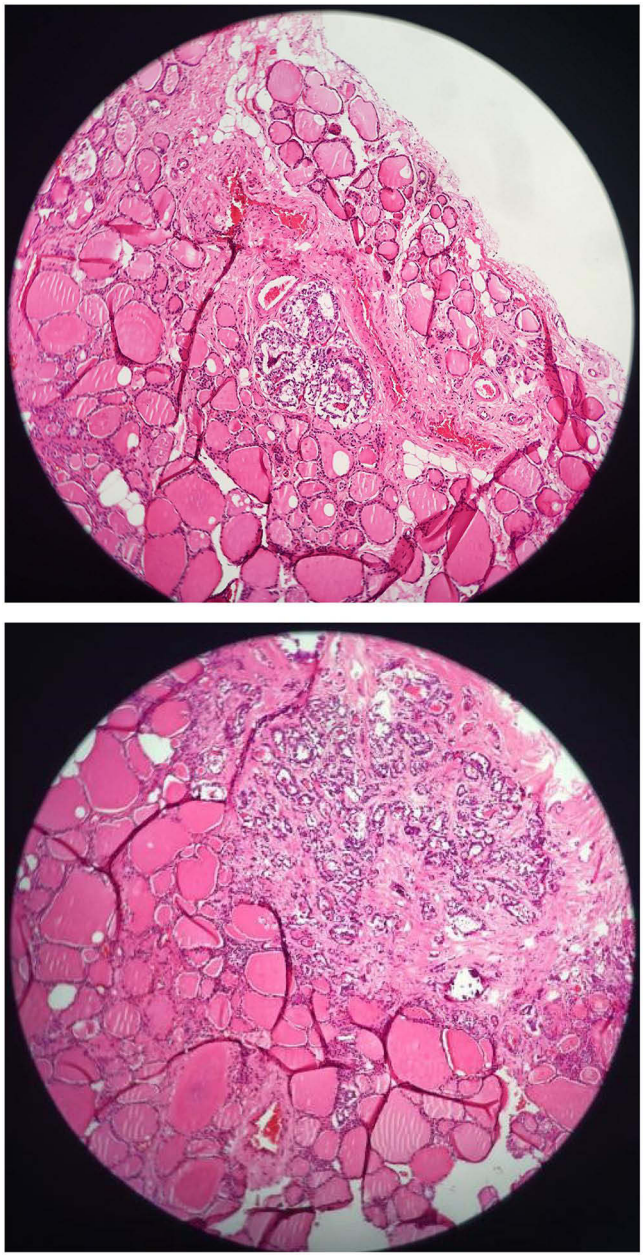

Figure 1 Histology result of PTC (10x). These tissues contains magnification fibrovascular centers, interstitial edema, eosinophilic cytoplasm, increased nucleus ratio, ground glass appearance, nuclear grooves and pseudoinclusion bodies in the nucleus, and thickened nuclear membrane.

Protein Identification Results

A total of 34420 peptides were identified, including 29835 unique peptides. A total of 5184 proteins were then identified, of which 5094 proteins could be quantitatively analyzed. We performed expression distribution (Figure 2) and correlation analysis (Figure 3) on the samples. The inter-group differences and intra-group repeatability can be evaluated from various perspectives. The median of the same group of samples in the box plot is close to the same horizontal line, and the histogram is close to the bell-shaped distribution. The closer the correlation is to 1, the better the data quality and repeatability.

Analysis of Differential Proteins in PTC

We further analyzed the 5094 proteins and classified proteins with a fold change (FC) greater than 1.2-fold (up- and downregulation) and P <0.05 in the pairwise comparison group as differentially expressed proteins. A total of 639 differentially expressed proteins were screened out, including 278 upregulated proteins and 361 downregulated proteins. A volcano map of differential expressed proteins was drawn using P-value and FC values to represent the distribution of differentially expressed proteins in cancer and para-carcinoma samples of PTC patients (Figure 4). We also performed cluster analysis on the differentially expressed proteins between cancer and adjacent normal tissues; the results showed that the protein expression levels were significantly different between the two groups (Figure 5).

GO Analysis of Differentially Expressed Proteins

To examine the functions of the differentially expressed proteins, we conducted GO analysis. Figure 6 lists the top 20 differentially expressed protein annotation results in different groups. Analysis of differentially expressed proteins in the biological process (BP) showed enrichments in drug metabolism, phylogeny, multicellular organism development, response to organic matter, cell response to chemical stimuli, regulation of cell component organization, organization of extracellular structures, organization of organelles, process of cell development, and assembly of cellular components. The molecular function (MF) of differentially expressed proteins mainly focused on binding activities, including enzyme binding, homotype protein binding, cell adhesion molecule binding, protein complex binding, receptor binding, cytoskeleton protein binding, and protein domain specific binding. The top 10 enriched terms in cellular components (CC) were dendritic tree, vesicles, cellular exosomes, extracellular organelles, cytoplasm, intracellular organelles, intracellular vesicles, intracellular part organelles, collagen-containing extracellular matrix and adherens junctions.

Pathway Analysis of Differentially Expressed Proteins

KEGG pathway enrichment analysis was performed on the differentially expressed proteins. A total of 281 pathways were annotated, of which 43 pathways were significantly enriched (Figure 7). Figure 8 shows the top 10 most

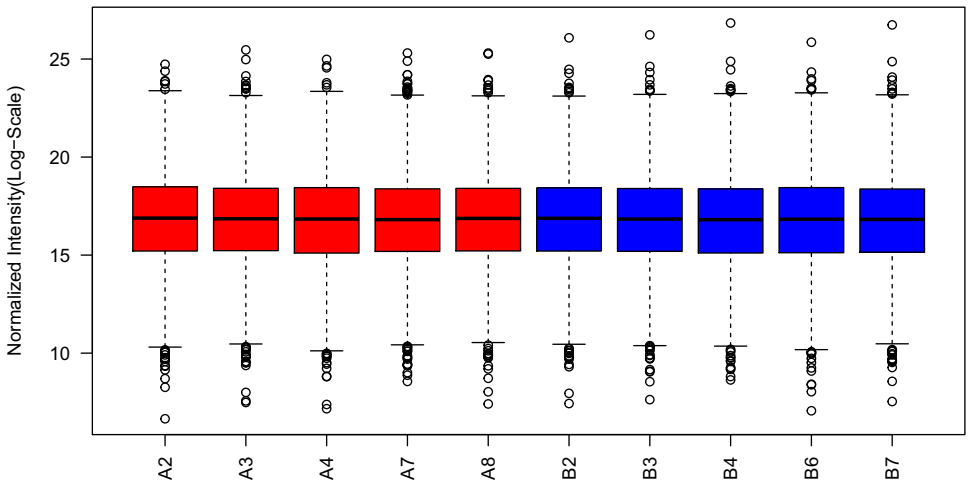

Figure 2 Distribution map of sample expression (box plot).

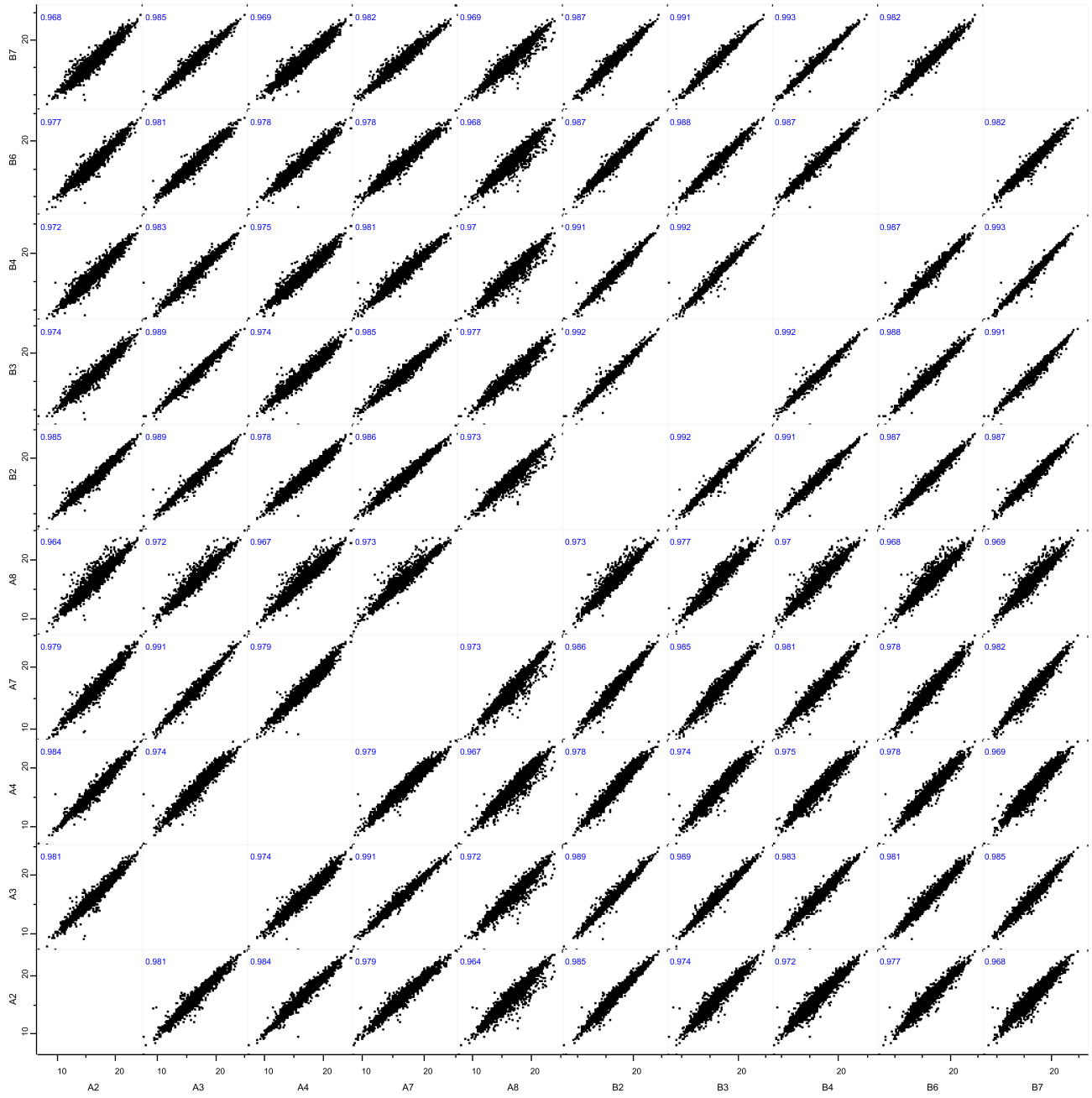

Figure 3 Correlation diagram of sample expression.

significantly enriched pathways; these included pathogenic *Escherichia coli* infection, extracellular matrix receptor interaction, mTOR signaling pathway, metabolic pathway, focal adhesion, thyroid hormone synthesis, leukocyte trans-endothelial migration, tight junctions, malaria, and cell adhesion molecules (CAMs). Among these pathways, the pathways related to thyroid cancer include extracellular matrix receptor interaction, mTOR signaling pathway, metabolic pathways, focal adhesions, thyroid hormone synthesis, leukocyte trans-endothelial migration, tight junctions, and CAMs.

Differentially Expressed Protein Function Interaction Network Analysis (PFIN)

We used the STRING database to construct a protein-protein interaction (PPI) network of the 639 differentially expressed proteins (Figure 9). The PPI network contained 634 nodes and 500 edges; the average node degree was 1.58, and the clustering coefficient was 0.321. The expected number of edges was 329. The expected value is significantly lower than

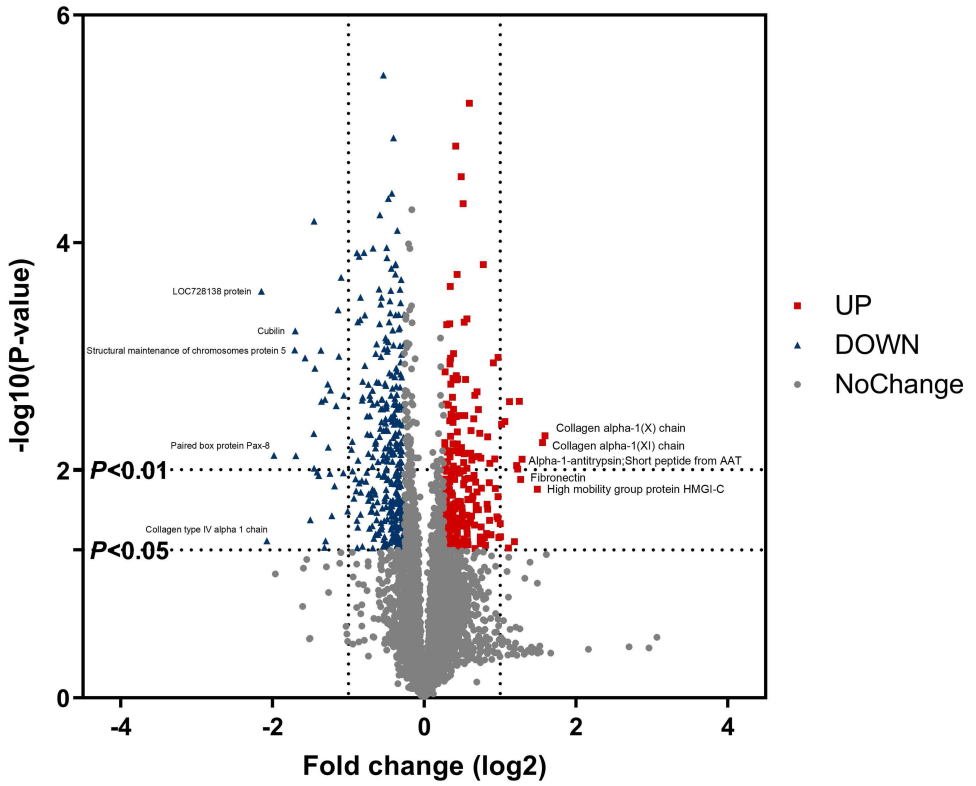

Figure 4 PTC differential protein volcano map. (**A**) cancer sample group, (**B**) para-cancerous sample group; the abscissa is the multiple of difference (logarithmic transformation with base 2), and the ordinate is the significance P value of the difference (logarithmic transformation with base 10). The red ones are up-regulated proteins, and the blue ones are down-regulated proteins.

the actual value, and the p-value of PPI enrichment is $< 1.0\times10^{-16}$. We imported the data into Cytoscape software and determined the top 10 hub proteins of the PPI network through the Maximum Clique Centrality (MCC) method of its extension program CytoHubba (Figure 10). The 10 hub proteins included Catenin beta-1 (CTNNB1), Cadherin-1 (CDH1), NADH dehydrogenase [ubiquinone] 1 alpha subcomplex subunit 9, mitochondrial (NDUFA9), NADH dehydrogenase [ubiquinone] 1 alpha subcomplex subunit 8 (NDUFA8), V-type proton ATPase catalyst tic subunit A (ATP6V1A), V-type proton ATPase subunit D (ATP6V1D), V-type proton ATPase subunit E 1 (ATP6V1E1), V-type proton ATPase subunit E 2 (ATP6V1E2), V-type proton ATPase subunit G 1 (ATP6V1G1), and V-type proton ATPase subunit C 1 (ATP6V1C1).

PRM Verification of Differential Proteins in PTC

Through GO functional enrichment analysis, we found that 533 differentially expressed proteins were annotated into the BP of activation. KEGG enrichment analysis revealed that 43 pathways were significantly enriched, and 201 differentially expressed proteins were annotated into these pathways. We performed Venn analysis on the 533 differentially expressed proteins corresponding to the activated/inhibited BP term and the 201 differentially expressed proteins in the KEGG enrichment results and identified 200 overlapping differentially expressed proteins (Figure 11). We conducted a literature search on the 200 differentially expressed proteins and selected 17 proteins that were most related to cancer. We then performed PRM verification to verify that the expression levels of these candidate proteins were consistent with the TMT-omics results. Eighteen proteins were subjected to PRM verification, and the results showed that the expression levels of all proteins were significantly different in thyroid subtissues and adjacent normal tissues (P<0.05) (Table 4).

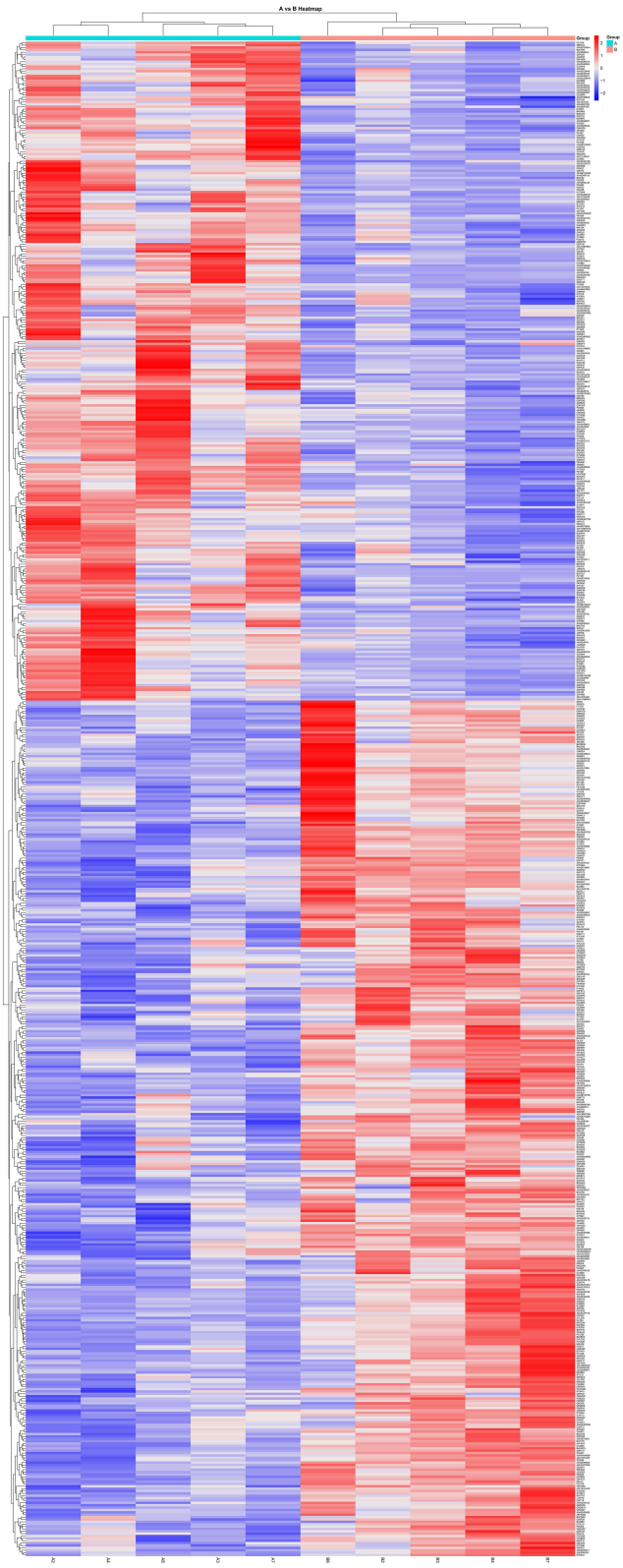

Figure 5 PTC differential protein clustering analysis heat map. (**A**) cancer sample group (**B**) para-cancerous sample group.

Discussion

Papillary thyroid carcinoma (papillary thyroid carcinoma) is a common endocrine tumor, and its incidence is increasing each year.[12] In the clinic, there are many benign thyroid diseases accompanied by obvious papillary hyperplasia that are

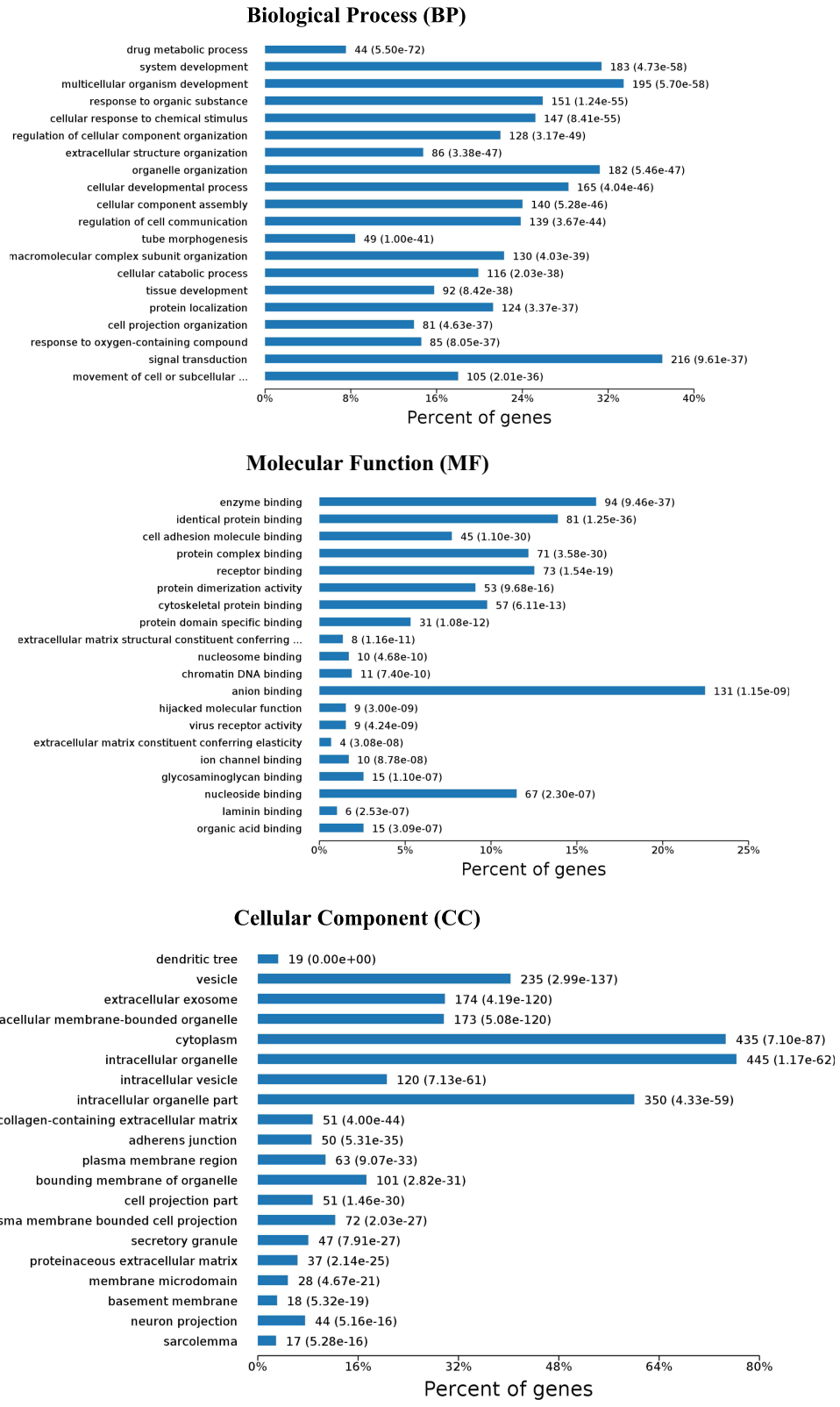

Figure 6 GO enrichment map of differentially expressed proteins.

Figure 7 KEGG enrichment pathway diagram of differentially expressed proteins.

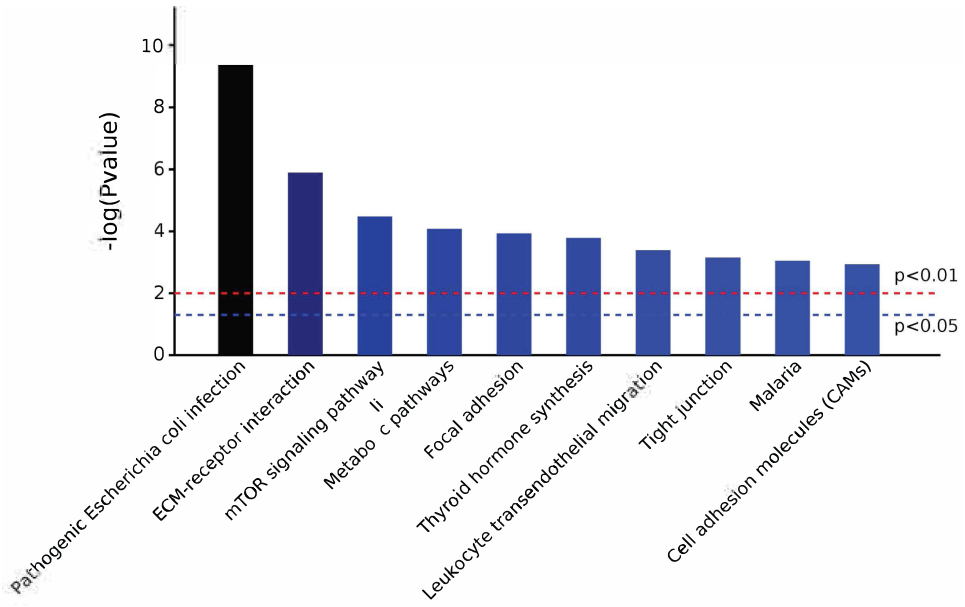

Figure 8 Bar chart of top 10 pathways in KEGG enrichment analysis of differentially expressed proteins.

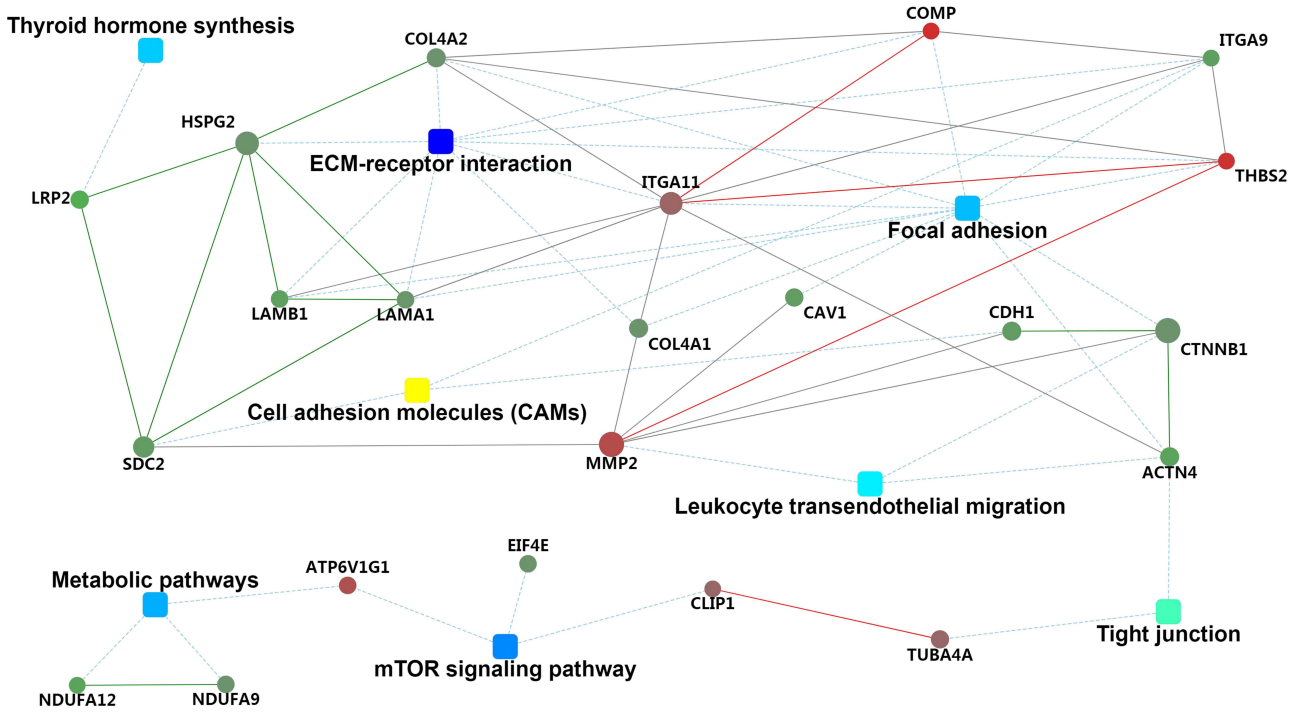

Figure 9 Overall PPI network of differentially expressed proteins constructed by STRING database.

difficult to distinguish from malignant tumor lesions and papillary hyperplasia, which leads to challenges in pathological detection or diagnosis. Therefore, identifying tumor-specific markers for papillary thyroid carcinoma will help clinicians more accurately and objectively judge the benign or malignant lesions of thyroid tumors, the clinical stage of malignant tumors, and the presence of metastatic lesions.

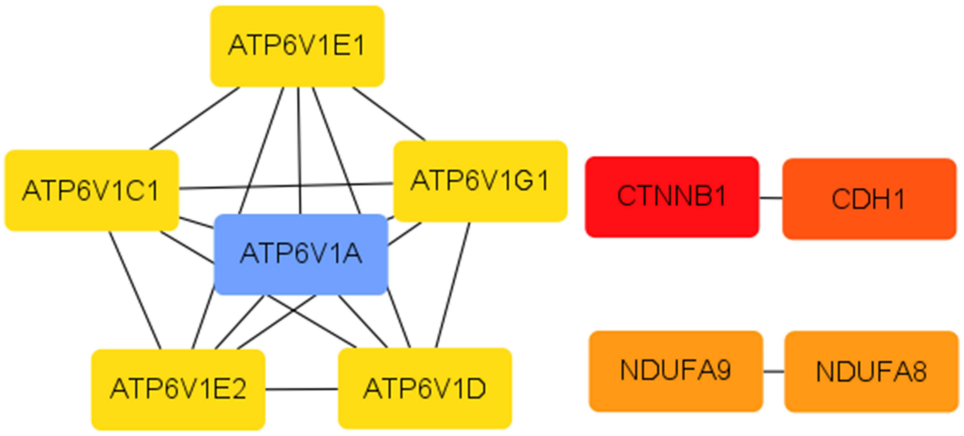

Figure 10 Using CytoHubba's MMC method to identify the top 10 proteins with the highest degree of PPI network connection.

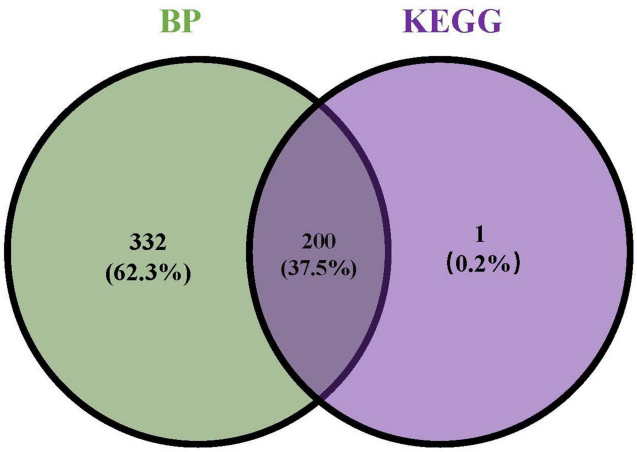

Figure 11 VENN diagram of common proteins in BP and KEGG.

Among the proteins and pathways screened in our study, other studies have also discovered the close relationship between THBS1, COMP and the mTOR pathway with papillary thyroid carcinoma and the mechanism of action of focal adhesion signaling pathway in medullary thyroid carcinoma. Regarding THBS1 and COMP proteins, we used a method distinct from those used in previous studies and established our results using proteomics; our findings are in line with

Table 4 PRM Verification Protein Expression Information

Protein Names	Protein NO.	Gene names	FC	P.value	PRM FC
Thrombospondin-2	A0A3B3ITK0	THBS2	1.960	0.017	135.143
Cartilage oligomeric matrix protein	G3XAP6	COMP	2.023	0.004	50.898
Collagen alpha-1(XII) chain	D6RGG3	COL12A1	1.821	0.009	27.451
Thrombospondin-1	A0A024R9Q1	THBS1	1.941	0.026	12.192
Persulfide dioxygenase ETHE1,	B2RCZ7	ETHE1	1.747	0.045	9.437
Chondroitin sulfate proteoglycan 2	A0A024RAQ9	CSPG2	1.963	0.001	7.614
BH3-interacting domain death agonist	B1PL87	BID	1.270	0.001	3.570
Apoptosis regulator BAX	Q07812	BAX	1.357	0.002	2.988
Adapter molecule crk	L7RT18	CRK	0.775	0.003	1.461
Filamin-B	O75369	FLNB	0.814	0.002	1.099

(*Continued*)

Table 4 (Continued).

Protein Names	Protein NO.	Gene names	FC	P.value	PRM FC
Catenin beta-1	B4DSW9	CTNNB1	0.804	0.032	0.961
Collagen alpha-1(IV) chain	Q59F15	COL4A1	0.807	0.019	0.877
Tenascin-X	A0A140T9C0	TNXB	0.780	0.041	0.853
Laminin subunit alpha-5	O15230	LAMA5	0.774	0.001	0.707
Hematopoietic progenitor cell antigen CD34	B4DG27	CD34	0.593	0.005	0.322
Thyroglobulin	P01266	TG	0.403	0.002	0.317
Carbonic anhydrase 4	P22748	CA4	0.365	0.000	0.130

previous results. THBS1 plays two main roles in tumors: inhibiting tumor angiogenesis and promoting tumor invasion and metastasis.[13,14] One study showed that high THBS1 expression is associated with higher TNM stage and malignancy, poorer prognosis, and higher recurrence rate of PTC.[15] The study used qPCR, immunohistochemistry and gene set enrichment analysis to demonstrate the up-regulation of THBS1 in PTC and its impact on prognosis. This approach is different from the proteomics methods used in our study, and each approach complements the other. In our study, we further verified the expression of THBS1 through PRM information, which enhances the reliability and integrity of the experimental results.

A previous study showed that the expression of COMP is high in PTC, and its expression is closely related to tumor size and lymph node metastasis.[16] COMP is mainly located in the cytoplasm of cells in PTC tissue.[17] High expression of COMP leads to enhanced invasion of cancer cells in PTC tissues to surrounding normal tissues and inhibits the apoptosis of cancer cells and changes cancer cell metabolism.[18] Some scholars use immunohistochemistry to silence COMP through lentiviral shRNA, perform RNA extraction, reverse transcription (RT)-PCR and real-time quantitative (qRT)-PCR, and determine the expression of the protein by measuring the gene that controls the production of the target protein. Another study showed that COMP promotes the development of tumors by regulating the release of intracellular calcitonin and oxidative phosphorylation of the endoplasmic reticulum.[19] Thus, expression of COMP in tumor cells leads to greater tumor spread and poorer prognosis. The results of this experiment verified and expounded the up-regulation of COMP in PTC tissue, and the magnitude was large, confirming its mechanism of action. We found that the expression of COMP is closely related to the focal adhesion signaling pathway, and this signaling pathway is involved in the expression of thyroid cancer and multiple other cancers. Therefore, our findings may provide a rationale for the role of COMP and focal adhesion signaling pathway in thyroid cancer.

This study is the first to examine the expression of other proteins in papillary thyroid carcinoma.

THBS2 is a disulfide-linked glycoprotein mainly produced by fibroblasts and smooth muscle cells that is involved in the late remodeling phase of tissue repair.[20] THBS2 regulates various biological processes such as angiogenesis, cell movement, and apoptosis by binding to extracellular matrix (ECM) proteins and cell surface receptors. Recent studies have shown that THBS2 also functions as both a proto-oncoprotein and a tumor suppressor. In colon cancer, THBS2 controls apoptosis by regulating the PI3K-AKT signaling pathway.[21] This pathway has also been confirmed to play an important role in PTC.[22] Other studies showed that THBS2 expression in colorectal cancer was positively correlated with multiple molecules in the Wnt/β-catenin signaling pathway, including β-catenin (CTNNB1), MMP-9 and cyclin D1. The Wnt/β-catenin signaling pathway is closely related to the occurrence of cancer. Our results identified CTNNB1 protein as one of the top 10 proteins with a higher degree of network connection, and interaction network analysis showed that THBS2 and CTNNB1 were co-enriched in the focal adhesion signaling pathway, which is closely related to PTC. Therefore, we speculate that THBS2 may play a role in the development of papillary thyroid carcinoma through specific and non-specific pathways. Future studies are required to explore this possibility.

Chondroitin sulfate proteoglycan 2 performs various functions such as cell adhesion, proliferation, migration and angiogenesis, and also plays a vital role in maintaining tissue morphogenesis. In bladder cancer, hypermethylation of CSPG2 is closely related to the muscle invasion of cancer cells and is related to tumor grade.[23–25] Furthermore, CSPG2 methylation indicates a higher risk of bladder cancer death.[26] However, the specific mechanism has not yet been found.

High expression of CSPG2 affects patient prognosis, and the current hypothesis is that CSPG2 controls the biological behavior of tumors by acting on the tumor microenvironment. No studies have examined on CSPG2 markers in thyroid cancer. Here we revealed the relationship between the up-regulation of CSPG2 expression and PTC, and the up-regulation fold also shows that this study has a certain accuracy. The role of CSPG2 in PTC needs further research and more study is required to determine whether CSPG2 has diagnostic value.

Collagen α-1(XII) (COL12A1) is an important extracellular matrix (ECM) protein that interacts with other molecules within the ECM[27] and plays a role in extracellular matrix maintenance and signal transduction between cells and the ECM. The ECM is a key component of the tumor microenvironment and regulates tumor invasion and migration.[28] Collagen includes 28 different isoforms and is the major insoluble fibrous protein in humans.[29] COL12A1 is highly expressed in colon cancer, and a higher expression is related to a poor prognosis. The two pathways most closely related to COL12A1 are the focal adhesion and PI3K-AKT pathways.[30] Our KEGG analysis results indicated that focal adhesion also plays a certain role in PTC. Some proteins, including COMP, which has been confirmed to be involved in PTC, THBS2 and CTNNB1, were enriched at various degrees in the focal adhesion pathway. The PI3K-AKT pathway is also a signaling pathway related to PTC.[31] Therefore, we speculate that COL12A1 regulates the occurrence and development of cancer through certain signaling pathways in various cancers. High expression of COL12A1 in PTC may also be from the activation of certain signaling pathways. Our study is the first to discover that the expression of COL12A1 chains is upregulated in papillary thyroid carcinoma. Follow-up studies are required to determine the mechanism and its diagnostic value, but the specificity of COL12A1 remains to be clarified.

The BH3-interacting domain death agonist (Bid) is a pro-apoptotic member of the B-cell lymphoma-2 (Bcl-2) protein family. Bid is sensitive to proteolytic cleavage by caspases, calpains, granzyme B, and cathepsins. Bid is extremely important for protease-mediated cell death and is involved in maintaining genome stability. Bid is the molecular linker that links various peripheral death pathways with the central mitochondrial pathway. Loss of Bid inhibits liver carcinogenesis, while Bid loss promotes tumorigenesis in myeloid cells.[32,33]

The three pathways most closely related to occurrence and development of PTC are the MAPK pathway, mTOR pathway, and PI3K-AKT pathway.[34–36] We compared the 22 pathways obtained by KEGG analysis with these pathways; our analysis showed that the PI3K-AKT pathway was changed in the process of chronic myeloid leukemia, and the Bid protein was up-regulated, participating in the formation of PTC. Bcl-2 participates in cell apoptosis. There are currently two mechanisms of apoptosis: the first is the way without the participation of Bcl family proteins. The second is the way Bcl family proteins participate, which is the biochemical pathway of cytochrome C release and activation of caspases, that is, the mitochondrial pathway. The Bcl protein family plays an important role in apoptosis. Bcl-2 protein inhibits the release of cytochrome C by preventing Bax from damaging the outer mitochondrial membrane.[37] When the expression of Bcl-2 increases, it forms a heterodimer with Bax, inhibits the production of Bax homodimers, and inhibits the release of cytochrome C, thereby exerting an anti-apoptotic effect. Bcl-2 prevents the redistribution of Bid, downregulates caspase-8, and inhibits cell death.[38] Bcl-2 interferes with the formation of death-inducing signaling complexes, prevents the translocation of Bax and Bid to mitochondria, and inhibits the activation of caspase-8.[39] Bcl-xL forms a ternary complex with Apaf-1 and caspase-9, which plays an anti-apoptotic role.[40] In response to ionizing radiation and genotoxic substances, Bcl-2 inhibits apoptosis by binding cytochrome C released from mitochondria into the cytoplasm to prevent the accumulation of cytochrome C. Through these mechanisms, Bcl-2 protein has several roles in cell apoptosis, suggesting the important role of Bid protein in cell apoptosis and its influence on tumorigenesis and development. How Bid is involved in PTC remains to be clarified, but Bid protein is expected to be a good molecular marker for PTC. KEGG analysis results suggested that Bid protein involvement in PTC may depend on the PI3K-AKT signaling pathway.

In addition, the results of differential protein interaction network analysis in this experiment show that among the top 10 proteins with the highest degree of PPI network connection identified by CytoHubba's MMC method, ATP6V1G1 is a hub protein connecting metabolic pathways and mTOR signaling pathways, and its expression was upregulated in PTC tissues. In our TMT results, we also found changes in NDFA protein family members, such as NDFA8 and NDFA9. However, NDFA9 and NDFA12, another family member, which play a role in the metabolic pathway, are downregulated in PTC tissue. Moreover, ITGA11 is the hub connecting extracellular matrix receptor interaction and focal adhesion. ITGA11 is also closely related to COMP and THBS2.

We used high-throughput proteomics technology for comprehensive and systematic screening and PRM technology for quantitative analysis and identified the following differentially expressed proteins: chondroitin sulfate proteoglycan 2 (chondroitin sulfate proteoglycan 2), collagen α-1 (XII) (COL12A1), cartilage oligomeric matrix protein, thrombospondin 1, BH3-interacting domain death agonist, and thrombospondin-2. These proteins may represent potential specific molecular marker for early screening of PTC and diagnostic standards for prognosis and recurrence. These results may even lead to find the identification of chemotherapy drugs for the treatment of PTC.

There are also other results found by other scholars on PTC and other thyroid carcinomas that may have some connections with the proteins and signal pathways of our findings. In a newly published meta-analysis article, they discovered that the Programmed Death-Ligand 1 (PD-L1) is related to chronic lymphocytic and BRAFV600E mutation status in PTCs. BRAF (BRAF mut) is the most common mutation in PTC (45% prevalence). In this study, it is confirmed that the association of PD-L1 and disease- free survival remained strong in PTC when compared with dedifferentiated thyroid carcinomas. However, the PD-L1 expression literally has no impact on mortality.[41] Our study also found some proteins and signal pathways closely related to BRAF V600E mutation.

However, there is a vital problem in the reservation of the tissues. PTCs have quite promising prognosis but it is relatively hard for longer following up. As to this situation, it is important to have good preservation of samples during time. It is believed that younger tissues contain more unique proteomics signals than the old ones.[42] The preservation environment of FFPE (formalin fixed paraffin embedding) blocks is very important for its preservation effect. In order to maintain the quality of FFPE blocks, environmental conditions need to be strictly controlled: 1. Temperature and humidity: The environment in which FFPE blocks are stored should be maintained at a temperature below 27°C and humidity between 30% and 70%. Excessive temperature and humidity will accelerate the aging and degradation of tissues, affecting the long-term stability of samples. 2. Prevention of parasite infestation: A system for parasite control should be in place to prevent damage to the sample. 3.Influence of fixed conditions: Formalin fixation may cause damage to antigens and trigger molecular cross-linking of proteins, resulting in a decline in the quality of subsequent antigen detection and molecular research. Therefore, a stable storage environment can minimize these effects and retain the original characteristics of the sample. In conclusion, preservation in line with the above environmental conditions can effectively slow down the degradation process of FFPE blocks and ensure the long-term validity and reliability of samples, which is crucial for future diagnosis and research.[43]

Conclusions

Using high-throughput proteomics technology for comprehensive and systematic screening and PRM technology for quantitative analysis, we identified chondroitin sulfate proteoglycan 2 (CSPG 2), collagen α-1 (XII) (COL12A1), cartilage oligomeric matrix protein (COMP), thrombospondin 1 (THBS1), BH3-interacting domain death agonist, and thrombospondin-2 as differential proteins in PTC. These findings may help lead to the identification of a specific molecular marker for early screening of PTC, a diagnostic standard for prognosis and recurrence and potential effective chemotherapy drugs for the treatment of PTC.

Summary Points

In this study, reliable PTC biomarkers, such as chondroitin sulfate proteoglycan 2 (CSPG 2), collagen α-1 (XII) (COL12A1), cartilage oligomeric matrix protein (COMP), thrombospondin 1 (THBS1), BH3-interacting domain death agonist, and thrombospondin-2 were screened by metabolic pathway analysis.

New PTC diagnostic methods can be established, the preoperative diagnosis rate of PTC was improved, the risk stratification system was improved, and individualized treatment was selected for patients, so as to achieve "accurate individualized treatment".

Multiple target proteins may become new molecular markers of thyroid papillary carcinoma by participating in multiple signaling pathways leading to the occurrence and development of papillary thyroid carcinoma.

Author Information

Yu Sun: ssssyy2000@126.com Jiaxuan Sun: Jorcy0709@163.com Xiaona Gao: 441198644@qq.com Tiefeng Shi: shitiefeng1970@163.com Maoqing Wang: wang_maoqing@126.com.

Ethical Disclosure

This study was approved by the ethics committee of The Second Affiliated Hospital of Harbin Medical University and all patients have signed informed consent. The manuscript of our study complies with the Declaration of Helsinki.

Acknowledgments

We thank Gabrielle White Wolf, PhD, from Liwen Bianji (Edanz) (www.liwenbianji.cn) for editing the English text of a draft of this manuscript.

Funding

This article is funded by financial assistance under Heilongjiang Postdoctoral Fund.

Disclosure

The authors report no conflicts of interest in this work. This paper has been uploaded to AUTHOREA as a preprint: https://doi.org/10.22541/au.170664054.44379830/v1.

References

1. Navas-Carrillo D, Ríos A, Rodríguez JM, Parrilla P, Orenes-Piñero E. Familial nonmedullary thyroid cancer: screening, clinical, molecular and genetic findings. *Biochim Biophys Acta*. 2014;1846:468–476. doi:10.1016/j.bbcan.2014.09.002
2. Cabanillas ME, McFadden DG, Durante C. Thyroid cancer. *Lancet*. 2016;388:2783–2795. doi:10.1016/S0140-6736(16)30172-6
3. Seib CD, Sosa JA. Evolving understanding of the epidemiology of thyroid cancer. *Endocrinol Metab Clin North Am*. 2019;48:23–35. doi:10.1016/j.ecl.2018.10.002
4. Li Y, Piao J, Li M. Secular trends in the epidemiologic patterns of thyroid cancer in china over three decades: an updated systematic analysis of global burden of disease study 2019 data. *Front Endocrinol*. 2021;12:707233. doi:10.3389/fendo.2021.707233
5. Omur O, Baran Y. An update on molecular biology of thyroid cancers. *Crit Rev Oncol Hematol*. 2014;90:233–252. doi:10.1016/j.critrevonc.2013.12.007
6. Zhang M, Luo Y, Zhang Y, Tang J. Efficacy and safety of ultrasound-guided radiofrequency ablation for treating low-risk papillary thyroid microcarcinoma: a prospective study. *Thyroid*. 2016;26(11):1581–1587. doi:10.1089/thy.2015.0471
7. Zhang M, Tufano RP, Russell JO, et al. Ultrasound-guided radiofrequency ablation versus surgery for low-risk papillary thyroid microcarcinoma: results of over 5 years' follow-up. *Thyroid*. 2020;30(3):408–417. doi:10.1089/thy.2019.0147
8. Yan L, Lan Y, Xiao J, Lin L, Jiang B, Luo Y. Long-term outcomes of radiofrequency ablation for unifocal low-risk papillary thyroid microcarcinoma: a large cohort study of 414 patients. *Eur Radiol*. 2021;31(2):685–694. doi:10.1007/s00330-020-07128-6
9. Chen J, Li XL, Zhao CK, et al. Conventional ultrasound, immunohistochemical factors and BRAF(V600E) mutation in predicting central cervical lymph node metastasis of papillary thyroid carcinoma. *Ultrasound Med Biol*. 2018;44(11):2296–2306. doi:10.1016/j.ultrasmedbio.2018.06.020
10. Liu H, Li Y, Mao Y. Local lymph node recurrence after central neck dissection in papillary thyroid cancers: a meta analysis. *Europ Annal Otorhinolaryngol Head Neck Dis*. 2019;136(6):481–487. doi:10.1016/j.anorl.2018.07.010
11. Deng L, Cao Y, Lin J. Regional recurrence rate of lymph-node-positive thyroid carcinoma after selective or comprehensive neck dissection. *Oral Oncol*. 2019;90:147–149. doi:10.1016/j.oraloncology.2018.11.034
12. Su Z, Yang Z, Xu Y, Chen Y, Yu Q. Apoptosis, autophagy, necroptosis, and cancer metastasis. *Mol Cancer*. 2015;14:48. doi:10.1186/s12943-015-0321-5
13. Zhang X, Huang T, Li Y, Qiu H. Upregulation of THBS1 is related to immunity and chemotherapy resistance in gastric cancer. *Int J Gen Med*. 2021;14:4945–4957. doi:10.2147/IJGM.S329208
14. Liu X, Xu D, Liu Z, et al. THBS1 facilitates colorectal liver metastasis through enhancing epithelial-mesenchymal transition. *Clin Transl Oncol*. 2020;22:1730–1740. doi:10.1007/s12094-020-02308-8
15. Abdullah MI, Junit SM, Ng KL, Jayapalan JJ, Karikalan B, Hashim OH. Papillary thyroid cancer: genetic alterations and molecular biomarker investigations. *Int J Med Sci*. 2019;16:450–460. doi:10.7150/ijms.29935
16. Wang N, Zhu L, Wang L, Shen Z, Huang X. Identification of SHCBP1 as a potential biomarker involving diagnosis, prognosis, and tumor immune microenvironment across multiple cancers. *Comput Struct Biotechnol J*. 2022;20:3106–3119. doi:10.1016/j.csbj.2022.06.039
17. Zhang J, Wang H, Lv C, et al. Cartilage oligomeric matrix protein affects the biological behavior of papillary thyroid carcinoma cells by activating the PI3K/AKT/Bcl-2 pathway. *J Cancer*. 2021;12:1623–1633. doi:10.7150/jca.49144
18. Englund E, Canesin G, Papadakos KS, et al. Cartilage oligomeric matrix protein promotes prostate cancer progression by enhancing invasion and disrupting intracellular calcium homeostasis. *Oncotarget*. 2017;8:98298–98311. doi:10.18632/oncotarget.21176
19. Rosas S, Hughes RT, Farris M, et al. Cartilage oligomeric matrix protein in patients with osteoarthritis is independently associated with metastatic disease in prostate cancer. *Oncotarget*. 2019;10:4776–4785. doi:10.18632/oncotarget.27113
20. Krady MM, Zeng J, Yu J, et al. Thrombospondin-2 modulates extracellular matrix remodeling during physiological angiogenesis. *Am J Pathol*. 2008;173:879–891. doi:10.2353/ajpath.2008.080128
21. Ao R, Guan L, Wang Y, Wang JN. Silencing of COL1A2, COL6A3, and THBS2 inhibits gastric cancer cell proliferation, migration, and invasion while promoting apoptosis through the PI3k-Akt signaling pathway. *J Cell Biochem*. 2018;119:4420–4434. doi:10.1002/jcb.26524
22. Shu C, Wang S, Hu J, et al. CircNDST1 promotes papillary thyroid cancer progression via its interaction with CSNK2A1 to activate the PI3K-Akt pathway and epithelial-mesenchymal transition. *J Endocrinol Invest*. 2023;46:545–557. doi:10.1007/s40618-022-01928-x

23. Maruyama R, Toyooka S, Toyooka KO, et al. Aberrant promoter methylation profile of bladder cancer and its relationship to clinicopathological features. *Cancer Res*. 2001;61(24):8659–8663.
24. Dudziec E, Goepel JR, Catto JW. Global epigenetic profiling in bladder cancer. *Epigenomics*. 2011;3(1):35–45. doi:10.2217/epi.10.71
25. Bilgrami SM, Qureshi SA, Pervez S, Abbas F. Promoter hypermethylation of tumor suppressor genes correlates with tumor grade and invasiveness in patients with urothelial bladder cancer. *SpringerPlus*. 2014;3:178. doi:10.1186/2193-1801-3-178
26. López JI, Angulo JC, Martín A, et al. A DNA hypermethylation profile reveals new potential biomarkers for the evaluation of prognosis in urothelial bladder cancer. *APMIS*. 2017;125(9):787–796. doi:10.1111/apm.12719
27. Sapudom J, Pompe T. Biomimetic tumor microenvironments based on collagen matrices. *Biomater Sci*. 2018;6(8):2009–2024. doi:10.1039/C8BM00303C
28. Jang I, Beningo KA. Integrins, CAFs and mechanical forces in the progression of cancer. *Cancers*. 2019;11(5):721. doi:10.3390/cancers11050721
29. Arseni L, Lombardi A, Orioli D. From structure to phenotype: impact of collagen alterations on human health. *Int J Mol Sci*. 2018;19(5):1407. doi:10.3390/ijms19051407
30. Wu Y, Xu Y. Integrated bioinformatics analysis of expression and gene regulation network of COL12A1 in colorectal cancer. *Cancer Med*. 2020;9(13):4743–4755. doi:10.1002/cam4.2899
31. Zheng T, Zhou Y, Xu X, et al. MiR-30c-5p loss-induced PELI1 accumulation regulates cell proliferation and migration via activating PI3K/AKT pathway in papillary thyroid carcinoma. *J Transl Med*. 2022;20(1):20. doi:10.1186/s12967-021-03226-1
32. Malkesman O, Austin DR, Tragon T, et al. Targeting the BH3-interacting domain death agonist to develop mechanistically unique antidepressants. *Mol Psychiatry*. 2012;17(8):770–780. doi:10.1038/mp.2011.77
33. Howells CC, Baumann WT, Samuels DC, Finkielstein CV. The Bcl-2-associated death promoter (BAD) lowers the threshold at which the Bcl-2-interacting domain death agonist (Bid) triggers mitochondria disintegration. *J Theor Biol*. 2011;271(1):114–123. doi:10.1016/j.jtbi.2010.11.040
34. Garnett MJ, Marais R. Guilty as charged: b-RAF is a human oncogene. *Cancer Cell*. 2004;6(4):313–319. doi:10.1016/j.ccr.2004.09.022
35. Nikiforov YE, Nikiforova MN. Molecular genetics and diagnosis of thyroid cancer. *Nature reviews*. *Endocrinology*. 2011;7(10):569–580. doi:10.1038/nrendo.2011.142
36. Lazaridis G, Lambaki S, Karayannopoulou G, et al. Prognostic and predictive value of p-Akt, EGFR, and p-mTOR in early breast cancer. *Strahlentherapie*. 2014;190(7):636–645. doi:10.1007/s00066-014-0620-6
37. Guedes JP, Baptista V, Santos-Pereira C, et al. Acetic acid triggers cytochrome c release in yeast heterologously expressing human Bax. *Apoptosis*. 2022;27(5–6):368–381. doi:10.1007/s10495-022-01717-0
38. Yang J, Liu X, Bhalla K, et al. Prevention of apoptosis by Bcl-2: release of cytochrome c from mitochondria blocked. *Science*. 1997;275(5303):1129–1132. doi:10.1126/science.275.5303.1129
39. Lutter M, Fang M, Luo X, Nishijima M, Xie X, Wang X. Cardiolipin provides specificity for targeting of tBid to mitochondria. *Nat Cell Biol*. 2000;2(10):754–761. doi:10.1038/35036395
40. Hu Y, Benedict MA, Wu D, Inohara N, Núñez G. Bcl-XL interacts with Apaf-1 and inhibits Apaf-1-dependent caspase-9 activation. *Proc Natl Acad Sci USA*. 1998;95(8):4386–4391. doi:10.1073/pnas.95.8.4386
41. Girolami I. Programmed Death-Ligand 1 (PD-L1) is a potential biomarker of disease-free survival in papillary thyroid carcinoma: a systematic review and meta-analysis of PD-L1 Immunoexpression in follicular epithelial derived thyroid carcinoma. *Endocrine Pathol*. 2020;31(3):291–300. doi:10.1007/s12022-020-09630-5
42. Eccher A, Seminati D, L'Imperio V, et al. Pathology laboratory archives: conservation quality of nucleic acids and proteins for NSCLC molecular testing. *J Pers Med*. 2024;14(4):333. doi:10.3390/jpm14040333
43. Eccher A, Scarpa A, Dei Tos AP. Impact of a centralized archive for pathology laboratories on the health system. *Pathol Res Pract*. 2023;245:245154488. doi:10.1016/j.prp.2023.154488